ChemRxiv™

Preprint

Design of supramolecular hybrid nanomaterials comprising peptide-based supramolecular nanofibers and *in situ* generated DNA nanoflowers through rolling circle amplification

Shintaro Sugiura[1], Yuki Shintani[1], Daisuke Mori[1], Sayuri L. Higashi[2], Aya Shibata[1], Yoshiaki Kitamura[1], Shin-ichiro Kawano[3], Koichiro M. Hirosawa[4], Kenichi G.N. Suzuki[4], Masato Ikeda[1,2,4,5]

[1]Department of Life Science and Chemistry, Graduate School of Natural Science and Technology, Gifu University, 1-1 Yanagido, Gifu 501-1193, Japan,

[2]United Graduate School of Drug Discovery and Medical Information Sciences, Gifu University, 1-1 Yanagido, Gifu 501-1193, Japan,

[3]Department of Chemistry, Faculty of Science, Nagoya University, Furo-cho, Chikusa-ku, Nagoya 464-8602, Japan,

[4]Institute for Glyco-core Research (iGCORE), Gifu University, 1-1 Yanagido, Gifu 501-1193, Japan,

[5]Institute of Nano-Life-Systems, Institutes of Innovation for Future Society, Nagoya University, Furo-cho, Chikusa-ku, Nagoya, 464-8603, Japan

*Correspondence: m_ikeda@gifu-u.ac.jp, orcid.org/0000-0003-4097-829

Table of contents

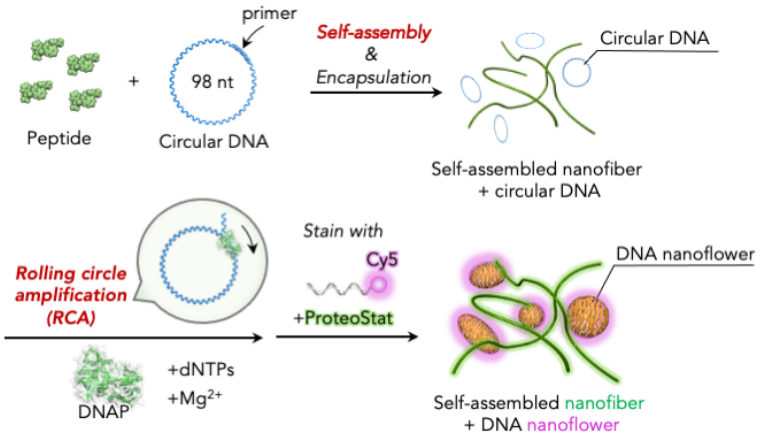

Keywords: DNA nanostructures • Peptide nanostructures • Self-assembly • Soft materials

Abstract

The artificial construction of multicomponent supramolecular materials comprising plural supramolecular architectures that are assembled orthogonally from their constituent molecules has attracted growing attention. Here, we describe the design and development of multicomponent supramolecular materials by combining peptide-based self-assembled fibrous nanostructures with globular DNA nanoflowers constructed by the rolling circle amplification reaction. The orthogonally constructed architectures were dissected by fluorescence imaging using the selective fluorescence staining procedures adapted to this study. The present, unique hybrid materials developed by taking advantage of each supramolecular architecture based on their peptide and DNA functions may offer distinct opportunities to explore their bioapplications as a soft matrix.

Introduction

Molecular assembly based on noncovalent synthesis has allowed the construction of various supramolecular nanostructures,[1,2,3] thereby helping in advancing our understanding of elaborate biological systems.[4] However, the artificial construction of multicomponent supramolecular materials comprising plural supramolecular architectures assembled exclusively and precisely from their constituent molecules has remained largely unexplored. In this context, because orthogonal self-assembly is of paramount importance, efforts to expand the repertoire of supramolecular architectures to meet the requirements for orthogonal self-assemblies have recently and actively been investigated.[5,6,7,8,9] Examples of aqueous multicomponent supramolecular materials include biomolecules like peptides and nucleic acids, which may be superlative candidates due to their potentially and tunable orthogonal molecular self-assembling propensities, biocompatibility, sustainability for future bioapplications, and availability.[10,11,12,13]

Rapidly expanding DNA nanotechnology has offered a bottom-up approach to access various supramolecular architectures with structural precision at nanometer and submicrometer scales, thereby eliciting controlled functions at the respective levels.[14,15,16] Accordingly, our previous study explored aqueous multicomponent supramolecular materials comprising semi-artificial glycopeptide-based self-assembled nanostructures, DNA microspheres,[17] and DNA tile nanotubes.[18] These DNA architectures were constructed through thermal annealing-induced hybridizations of multiple and sequence-programmed nucleic-acid chains (typically, three DNA-microsphere strands [19,20] and five DNA tile nanotube strands [21]). Meanwhile, rolling circle amplification (RCA) has attracted growing attention as an isothermal enzymatic process to obtain DNA-based nanostructures and microstructures.[22,23] Notably, for example, under typical RCA conditions in the presence of divalent cations such as the magnesium ion, unique globular and flower-like morphology (referred to as DNA nanoflowers) emerge spontaneously as RCA products. These products most presumably arise through the complexation of the as-synthesized long single-stranded (ss) DNA molecules with divalent cationic pyrophosphate (e.g., Mg_2PPi).[24] However, to our knowledge, the orthogonal coexistence of

DNA nanoflowers as RCA products and peptide-based supramolecular nanostructures had not been investigated yet.

We herein describe the construction of multicomponent supramolecular materials by combining peptide-based self-assembled fibrous nanostructures and DNA nanoflowers constructed by the RCA reaction. As depicted in **Fig. 1**, circular DNA molecules could be entrapped inside a network of peptide-based self-assembled fibrous nanostructures. Then, subsequent isothermal RCA reactions catalyzed by DNA polymerase (DNAP) could give rise to the *in situ* formation of DNA nanoflowers in the presence of peptide-based self-assembled fibrous nanostructures. In this study, we focused on investigating self-assembled nanostructures constructed from newly designed and synthesized anionic peptide derivatives and constructing hybrid materials by combining them with DNA nanoflowers. We expect that the developed unique hybrid materials could offer distinct opportunities to explore their bioapplications as soft matrices by taking advantage of the functions of each supramolecular architecture.

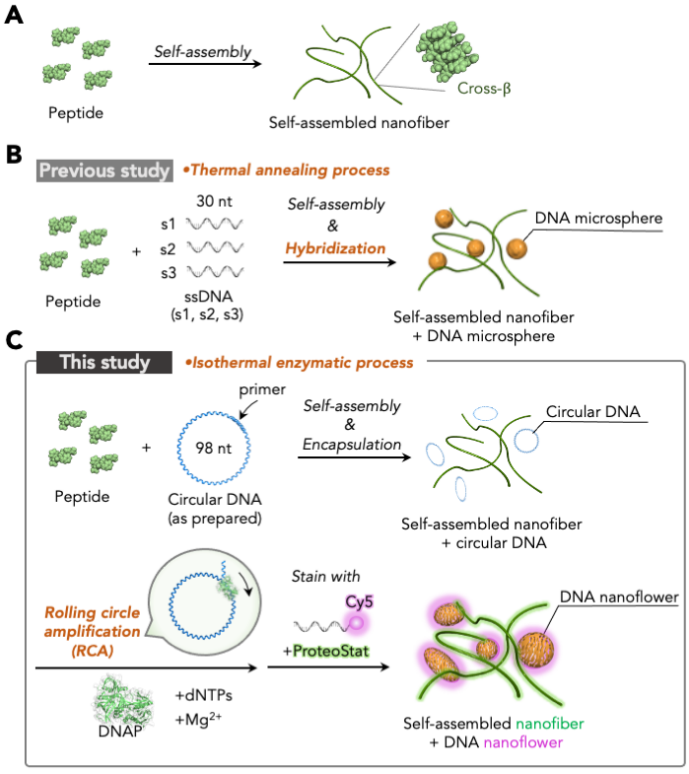

Fig. 1 Schematic (not to scale) showing (**A**) self-assembly of peptides to form fibrous supramolecular (self-assembled) nanostructures, (**B**) an orthogonal construction of hybrid materials comprising peptide-based self-assembled nanofibers and DNA microspheres through the thermal annealing process [17], and (**C**) the isothermal enzymatic construction of DNA nanoflowers through RCA in the presence of peptide-based self-assembled nanofibers, giving rise to hybrid materials.

Results and discussion

Synthesis and hydrogel formation abilities of the anionic peptide derivatives

In this study, we newly designed two anionic peptide derivatives (**Z-AF-BPS** and **Z-FA-BPS**, **Fig. 2A**), comprising phenylalanine (F) and alanine (A). Their syntheses were carried out according to **Scheme S1** modified slightly from our previous report on the similar compound.[25] As shown in **Fig. 2B**, **Z-AF-BPS** showed hydrogel formation abilities above 0.40 wt% (6.4 mM) whereas no hydrogel formation was observed with its inversed sequence (**Z-FA-BPS**), even at a higher concentration such as 1.0 wt% (15 mM) and after 24-h incubation. In the following studies, we investigated the properties of **Z-AF-BPS** hydrogel because the formation of a self-assembled nanostructure network was reasonably anticipated for the **Z-AF-BPS** hydrogel.

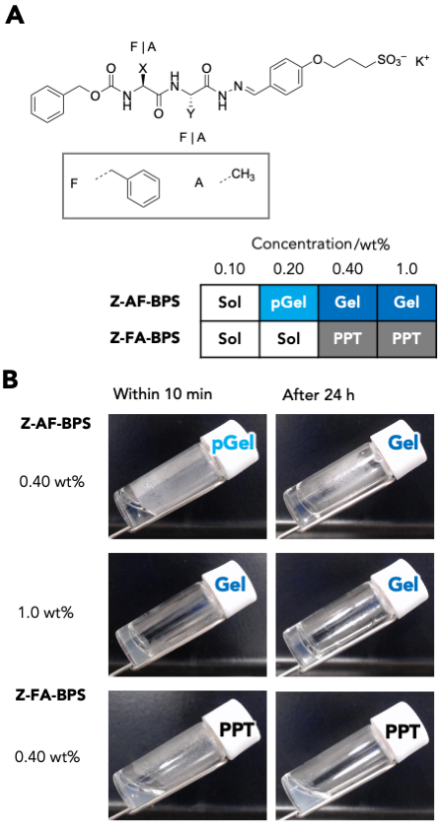

Fig. 2 (**A**) Chemical structures of the self-assembling peptides (**Z-AF-BPS** and **Z-FA-BPS**) designed and synthesized in this study, showing their gel formation abilities based on their concentrations [Sol: solution, pGel: partial gel, Gel: gel, and PPT: precipitation (or suspension)]. (**B**) Photographs showing **Z-AF-BPS** hydrogels and **Z-FA-BPS** suspensions obtained 10 min and 24 h after dissolution by heating [**Fig. S9A** shows photographs of the other conditions in panel (**A**)]. *Conditions*: 50 mM MES-NaOH (pH 7.0) containing DMSO (2.0 vol%).

Characterization of the Z-AF-BPS hydrogel

Viscoelastic properties of the **Z-AF-BPS** hydrogel was evaluated by rheology measurements. Although an almost linear viscoelastic region was uncovered by strain sweep oscillatory rheology, the mechanical weaknesses of the hydrogel were evident from its relatively low storage (G') and loss modulus (G'') compared with similar peptide-based hydrogels (**Fig. S10**).[25] Microscopic observations were subsequently conducted to gain insight into the self-assembled structures of **Z-AF-BPS**. As shown in **Fig. 3A**, the atomic force microscopy

(AFM) images (under ambient air conditions) revealed long straight nanofibers with a length over several μm and an average height of 3.4 nm. The formation of such extended one-dimensional self-assembled architectures would be attributed to the hydrogel formation ability of **Z-AF-BPS**. Nevertheless, the weak entanglement of the nanofibers, most probably due to electrostatic repulsion, could be correlated with the mechanical weakness of the hydrogel. On the other hand, the smooth fibrous structures with the height (3.4 nm), which is less than the double of the molecular length (2.6 nm) of **Z-AF-BPS**, suggest the interdigitated bimolecular structure as a unit for the one-dimensional self-assembled structure. A plausible model for the self-assembled **Z-AF-BPS** structure displayed as **Fig. 3B** may be explained, at least in part, as a weak entanglement and bundling of the negatively charged nanofibers through electrostatic repulsion, which would be desirable for the orthogonal coexistence with other supramolecular architectures in aqueous media, owing to mitigated nonspecific interactions that produce undesired and less-controlled aggregations. Transmission electron microscopy (TEM) image (*vide infra*) results disclose the comparable thin long nanofibers.

Subsequently, we gained further insight into the molecular assembly mode of **Z-AF-BPS** to form fibrous architectures by X-ray diffraction (XRD) measurements. To this end, freeze-dried xerogel samples were prepared from hydrogels using deionized water instead of the aqueous buffer [50 mM MES-NaOH (pH 7.0)] because the aqueous buffer contains salts that potentially interfere with the XRD data and was unremovable. Almost comparable hydrogel formation abilities were validated under both conditions (**Fig. S9B**). As shown in **Fig. 3C**, we observed that a broad peak centered as the Bragg spacing at d = 4.6 Å (peak #5), which is assignable to the inter-strand distance of the β-sheet structure. We also observed a shoulder peak at d = 3.9 Å (peak #6), probably assignable to the π–π stacking of the aromatic groups in phenylalanine (F) as well as the Z and BPS moieties in **Z-AF-BPS**. These findings were consistent with the cross-β structure [26] for **Z-AF-BPS** nanofibers. Additionally, a weak but distinguishable peak at d = 9.6 Å (peak #4), most probably ascribed as the inter-sheet stacked distance of the β-sheet structure for a typical cross-β structure, was observed. Furthermore, a peak was observed at a small angle region, d = 48 Å (peak #1), which was presumably accompanied by higher-order reflections [d = 24 Å (peak #2) and 16 Å (peak #3)]. These diffractions suggest that **Z-AF-BPS** self-assembled to form a layer structure with a spacing of 4.8 nm in the xerogel (dried) state, meaning probably a lateral bundling of **Z-AF-BPS** nanofibers. Moreover, the spacing of 4.8 nm, most likely ascribed to the diameter of **Z-AF-BPS** nanofibers, was shorter than double the molecular length (2.6 nm) and the height (3.4 nm) of the fibrous structures observed in the AFM images, in which a tip- and/or surface-induced deformation should be considered.[27,28] Collectively, these XRD results indicate the interdigitated bimolecular and cross-β structure of **Z-AF-BPS** nanofibers (**Fig. 3B**) while tilting the β-strand against the long axis of the fibers was also conceivable.[29]

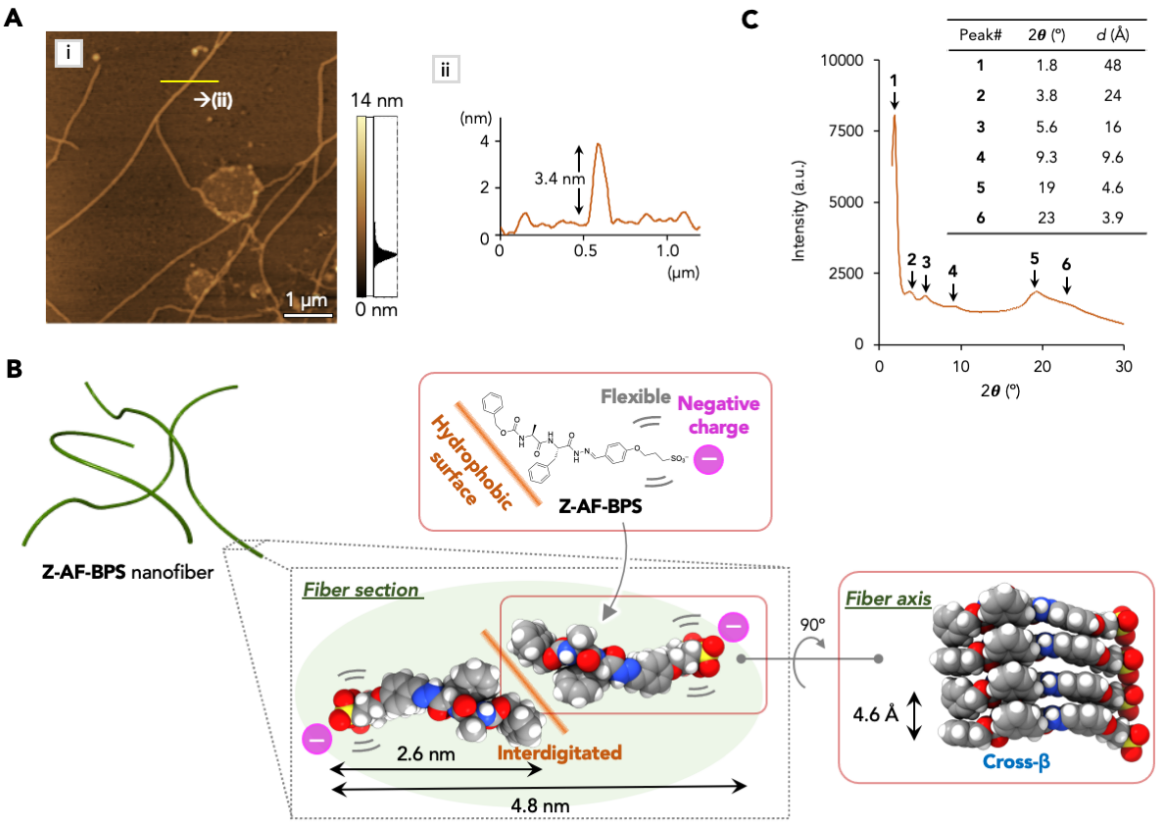

Fig. 3 (**A**) Representative AFM (tapping mode) images showing the height image (**i**) of **Z-AF-BPS** nanofibers on freshly cleaved mica. The panel (**ii**) represents a cross-sectional profile along the white line in the image (**i**). (**B**) Plausible models for the self-assembled structure of **Z-AF-BPS**, giving rise to one-dimensional (cross-β) bimolecular structures in the hydrogel state. (**C**) XRD pattern from a freeze-dried sample of **Z-AF-BPS** hydrogel (1.0 wt%).

Spectroscopic studies on the Z-AF-BPS hydrogel

Fig. 4A shows a circular dichroism (CD) spectrum of the **Z-AF-BPS** hydrogel (0.40 wt%, 6.4 mM) exhibited a negative CD signal at 310 nm, assignable to a chiral arrangement of BPS moiety in the self-assembled fibrous structures that can be originated from chiral information transfer from peptide moiety to BPS moiety enhanced by self-assembly.[25] Furthermore, a positive CD signal at 240 nm and a negative CD signal shorter than 235 nm were observed. In this wavelength region (200–250 nm), the presence of phenylalanine (F) as well as the Z and BPS moieties in **Z-AF-BPS** could lead to a mixed spectra ascribable to the electronic transitions of its peptide backbone and aromatic moieties.[25,30] The CD signals became almost silent at a lower concentration (0.040 wt%, 0.64 mM), indicating the absence of self-assembled structures at the lower concentration. Indeed, the thioflavin T (ThT) assay conducted under similar conditions revealed that critical aggregation concentration of **Z-AF-BPS** was 0.73 ± 0.03 mM (n = 3; **Fig. S11**). Fourier-transform infrared (FTIR) spectra of **Z-AF-BPS** hydrogel exhibited two major bands centered at 1639 and 1686 cm^{-1} with shoulder peaks as displayed in **Fig. 4B**, suggesting that hydrogen bonding of an amide backbone and (Z-related) carbonate moieties at the N-terminal

via β-sheet formation, consistent with the proposed self-assembled structure depicted in **Fig. 3B**.

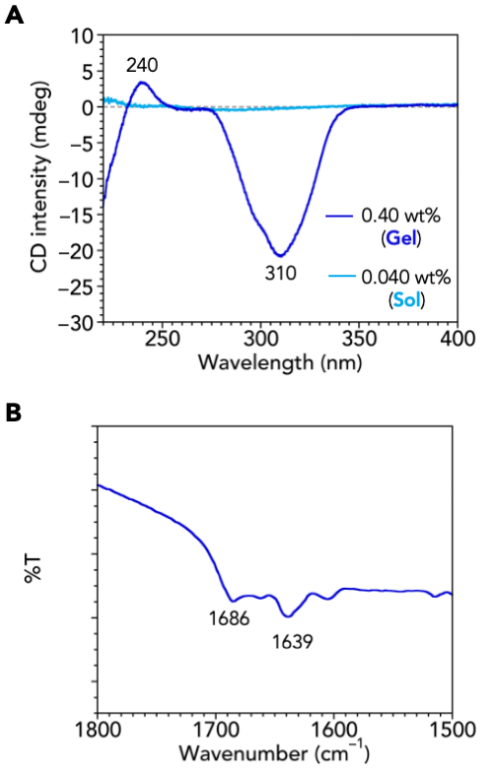

Fig. 4 (**A**) CD spectra of the **Z-AF-BPS** hydrogel (0.40 wt%, 0.1-mm cell) and sol (0.040 wt%, 1.0-mm cell). *Conditions*: 50 mM MES-NaOH (pH 7.0) containing DMSO (2.0 vol%). (**B**) IR spectrum of the **Z-AF-BPS** hydrogel [5.0 wt%, prepared with D_2O (**Fig. S9B**) to detect the bands in the amide I region].

Isothermal enzymatic construction of DNA nanoflowers through RCA in the presence of peptide-based self-assembled nanofibers

Next, we envisioned the isothermal enzymatic construction of aqueous hybrid materials by mixing the newly developed, negatively charged **Z-AF-BPS** nanofibers with the DNA nanoflowers that were obtained as RCA products. Notably, selective fluorescent staining dyes for each supramolecular architecture are indispensable to visualizing **Z-AF-BPS** nanofibers and DNA nanoflowers individually and in their mixed states through *in situ* confocal laser scanning microscopy (CLSM) observations.[31] In this study, ProteoStat [32], a commercially available fluorescent molecular rotor dye (lacking an open chemical structure) for staining amyloid plaques, was used to stain **Z-AF-BPS** nanofibers because of its robust selectivity demonstrated during the intracellular fluorescence imaging of peptide-based aggregates, as reported by other groups.[33,34] Then, a fluorescent-dye-labeled oligonucleotide (Cy5-ON, 12 nt), having a complementary sequence to an ssDNA part (which repeatedly appears) and constructed by an RCA reaction, was employed to visualize DNA nanoflowers according to previous reports.[35,36]

As shown in **Fig. 5Aii**, a fibrous morphology was observed using the ProteoStat green channel for **Z-**

AF-BPS nanofibers while **Fig. 5Bi** showed the successful observation of a particulate morphology under a Cy5 magenta channel for DNA nanoflowers obtained by the RCA, according to the standard procedure reported previously (incubation was conducted at room temperature (rt, ~25 ºC) for 4 h).[37,38] As the RCA template, a circular DNA (98 nt) was prepared, the formation of which was verified by PAGE (**Fig. S12**) and directly applied to the RCA reaction according to the previous report.[38] TEM observations of the RCA reaction products (*vide infra*) disclosed the formation of globular DNA nanoflowers, consistent with previous reports.[37,38] Most importantly, we found that the nonspecific staining was insignificant (**Fig. 5Ai**: Cy5-ON against **Z-AF-BPS** nanofibers, **5Bii**: ProteoStat against DNA nanoflowers) and supported by the low Pearson's correlation coefficient (PCC) values displayed in the merged channels (**Fig. 5Aiii** and **5Biii**).

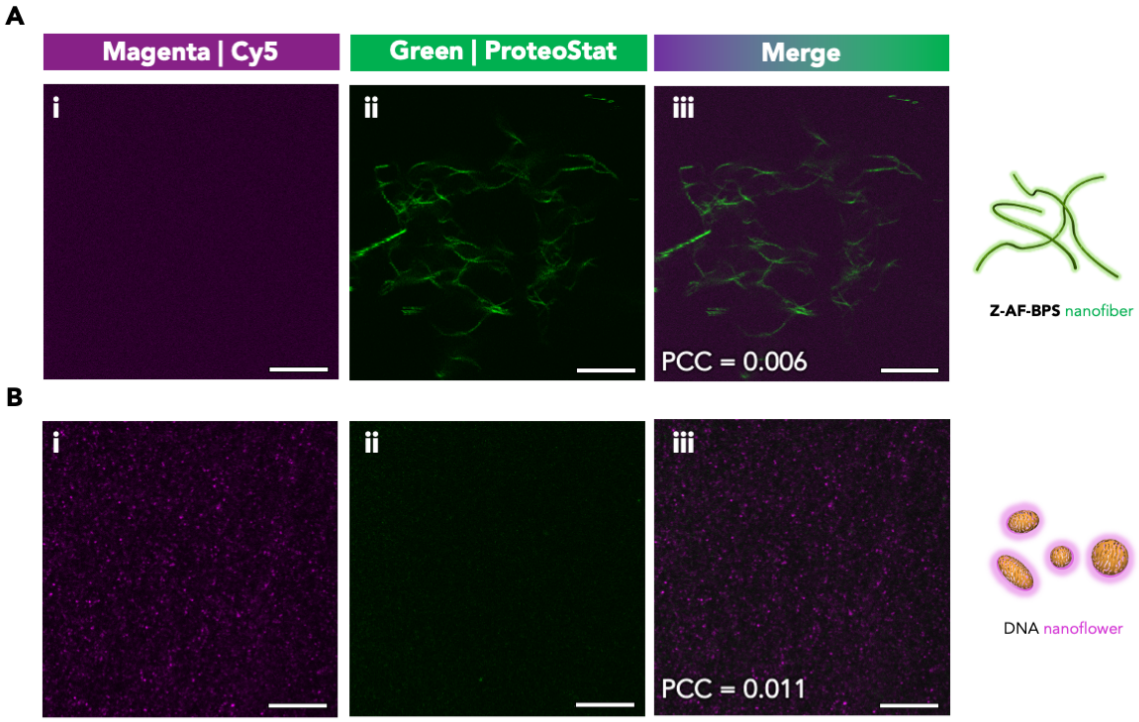

Fig. 5 Representative CLSM images showing (**A**) **Z-AF-BPS** nanofibers and (**B**) DNA nanoflowers obtained by the RCA and subsequently stained with ProteoStat and Cy5-ON. Details on sample preparation and CLSM observation procedures are described in the supplementary information. Scale bar: 10 μm. *Conditions*: (**A**) [**Z-AF-BPS**] = 8.2 mM, (**B**) [dNTPs] = 1.0 mM and [DNAP] = 1000 U/mL, staining with ProteoStat (1/500 dilution of the ProteoStat staining solution) and Cy5-ON (16 μM).

Next, two protocols were designed to establish procedures for constructing new hybrid materials comprising **Z-AF-BPS** nanofibers and DNA nanoflowers. As outlined in **Fig. 6A**, pregrown DNA nanoflowers (typically at rt for 4 h) were mixed with a small amount of DMSO stock solution containing monomeric **Z-AF-BPS** to induce the formation of the **Z-AF-BPS** nanofibers for (i) the post-RCA-mixing protocol. In contrast, the RCA reaction (conducted at rt for 4 h) was performed to grow DNA nanoflowers in the presence of **Z-AF-BPS** nanofibers for (ii) the pre-RCA-mixing protocol (**Fig. 7A**). First, the hybrid materials prepared according

to (i) the post-RCA-mixing protocol were subjected to CLSM observations through the above-described fluorescence staining method. As shown in **Fig. 6B**, fibrous morphology in the green channel and particulate morphology in the magenta channel were individually observed, indicating the orthogonal coexistence of **Z-AF-BPS** nanofibers and DNA nanoflowers obtained from the RCA reaction before the mixing. The PCC value was evaluated to be 0.284, indicating an appreciably low correlation between the green and magenta channels. Encouraged by this selective fluorescence staining results, even under the mixed state, we subsequently prepared hybrid materials according to (ii) the pre-RCA-mixing protocol, which was, in fact, our original purpose as depicted in **Fig. 1C**. As displayed in **Fig. 7B**, CLSM images comparable to those in (ii) the pre-RCA-mixing protocol were obtained, the PCC value (0.475) was larger, a possible reason of which will be discussed later. Nonetheless, this finding indicates that RCA reactions in the presence of **Z-AF-BPS** nanofibers orthogonally proceeded to allow for the *in situ* production of DNA nanoflowers, which manifests the successful, isothermal enzymatic construction of multicomponent supramolecular hybrid materials containing two distinct supramolecular architectures (nanofibers and nanoflowers) assembled from their component peptides and nucleic acids, respectively.

Subsequently, proteinase K [39] was added to the hybrid materials constructed according to the two distinct protocols to evaluate biostimuli responsiveness and further dissect the orthogonal coexistence of the DNA nanoflowers and **Z-AF-BPS** nanofibers.[17,18] We observed that although the fibrous morphology visualized by the ProteoStat green channel disappeared almost entirely after 16-h incubation at 40 ºC in the presence of proteinase K, the particulate morphology in the Cy5 magenta channel remained as shown in **Figs. 6C** and **7C**. As anticipated, the selective degradation of the **Z-AF-BPS** nanofibers by proteinase K was evident. Furthermore, this protease-selective degradation supports our view that fibrous architectures visualized by CLSM observations can be constructed orthogonally from peptide derivatives (**Z-AF-BPS**) against the DNA-based globular architectures.

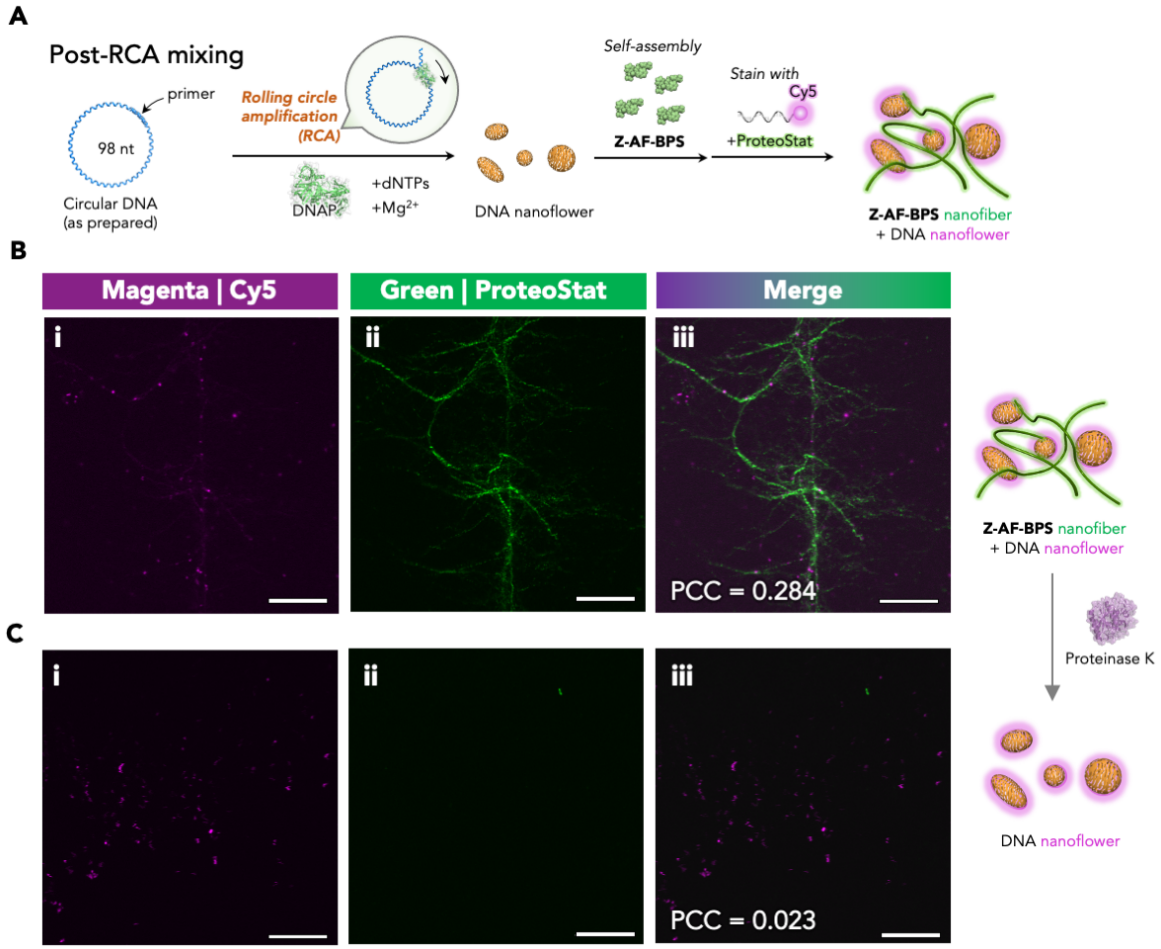

Fig. 6 (**A**) The post-RCA-mixing protocol to construct hybrid materials comprising **Z-AF-BPS** nanofibers and DNA nanoflowers. Representative CLSM images of the **Z-AF-BPS** nanofibers and DNA nanoflowers were shown by staining with ProteoStat and Cy5-ON, respectively, (**B**) before and (**C**) after adding proteinase K (11 mg/mL). Details on the sample preparation and CLSM observation procedures are described in the supplementary information. Scale bar: 10 μm. *Conditions*: (**B**) [**Z-AF-BPS**] = 8.2 mM, [dNTPs] = 1.0 mM, and [DNAP] = 1000 U/mL, staining with ProteoStat (1/500 dilution of the ProteoStat staining solution) and Cy5-ON (16 μM).

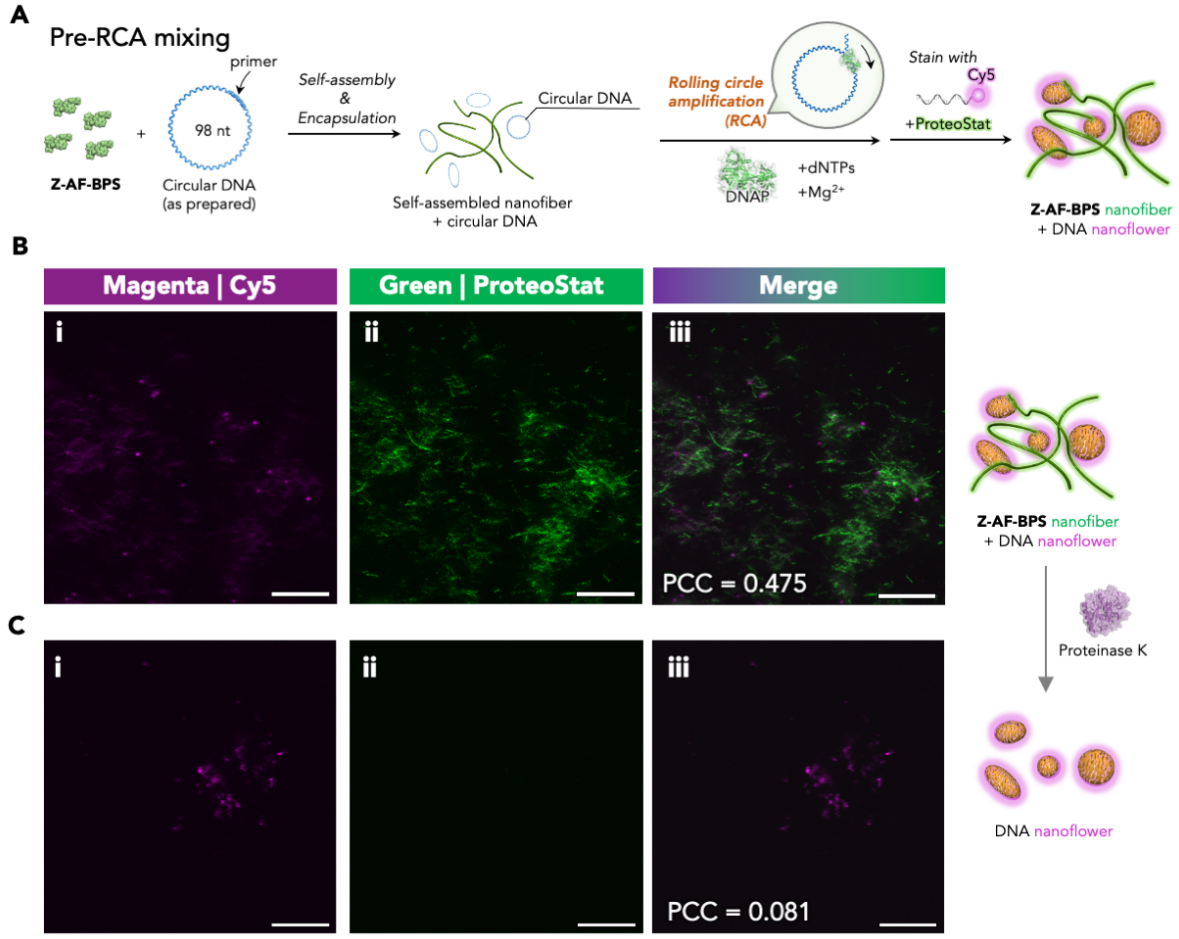

Fig. 7 (**A**) The pre-RCA-mixing protocol to construct hybrid materials comprising the **Z-AF-BPS** nanofibers and DNA nanoflowers. Representative CLSM images of the **Z-AF-BPS** nanofibers and DNA nanoflowers were shown by staining with ProteoStat and Cy5-ON, respectively, (**B**) before and (**C**) after adding proteinase K (11 mg/mL). Details on the sample preparation and CLSM observation procedures are described in the supplementary information. Scale bar: 10 μm. *Conditions*: (**B**) [**Z-AF-BPS**] = 8.2 mM, [dNTPs] = 1.0 mM, and [DNAP] = 1000 U/mL, staining with ProteoStat (1/500 dilution of the ProteoStat staining solution) and Cy5-ON (16 μM).

Finally, TEM observations were conducted to obtain further insight into the orthogonal coexistence of **Z-AF-BPS** nanofibers and DNA nanoflowers at a nanoscale. As shown in **Fig. 8A**, long thin nanofibers with a length of several μm and a diameter of several nm were discovered. Notably, the **Z-AF-BPS** nanofibers found in these TEM images were significantly thin and scarcely entangled compared with those of the supramolecular nanofibers constructed from the similar peptide derivatives reported previously by our group [25]. Hence, the fibrous morphology coincided with the AFM images (**Fig. 3A**). More importantly, aggregated DNA nanoflowers were often found along with **Z-AF-BPS** nanofibers (**Fig. 8B**). This structural nanoscale feature could be correlated with marginally larger PCC values for the CLSM images (**Fig. 7B**). Moreover, although the sizes of the individual DNA nanoflowers (ca. 50–200 nm) were comparable to those reported previously,[37,38,40,41]

they were more polydisperse. In contrast, as shown in **Fig. 8C**, less aggregated DNA nanoflowers, with the size of 72 ± 18 nm (n = 190), were found in the absence of **Z-AF-BPS** nanofibers. Therefore, we presume that the aggregation of DNA nanoflowers found frequently along with the **Z-AF-BPS** nanofibers could be facilitated by attractive interactions between DNA nanoflowers and the **Z-AF-BPS** nanofibers and/or the surface of **Z-AF-BPS** nanofibers could act as a template for the growth of DNA nanoflowers,[18] which could be mediated by a divalent cation (Mg^{2+} under this conditions).

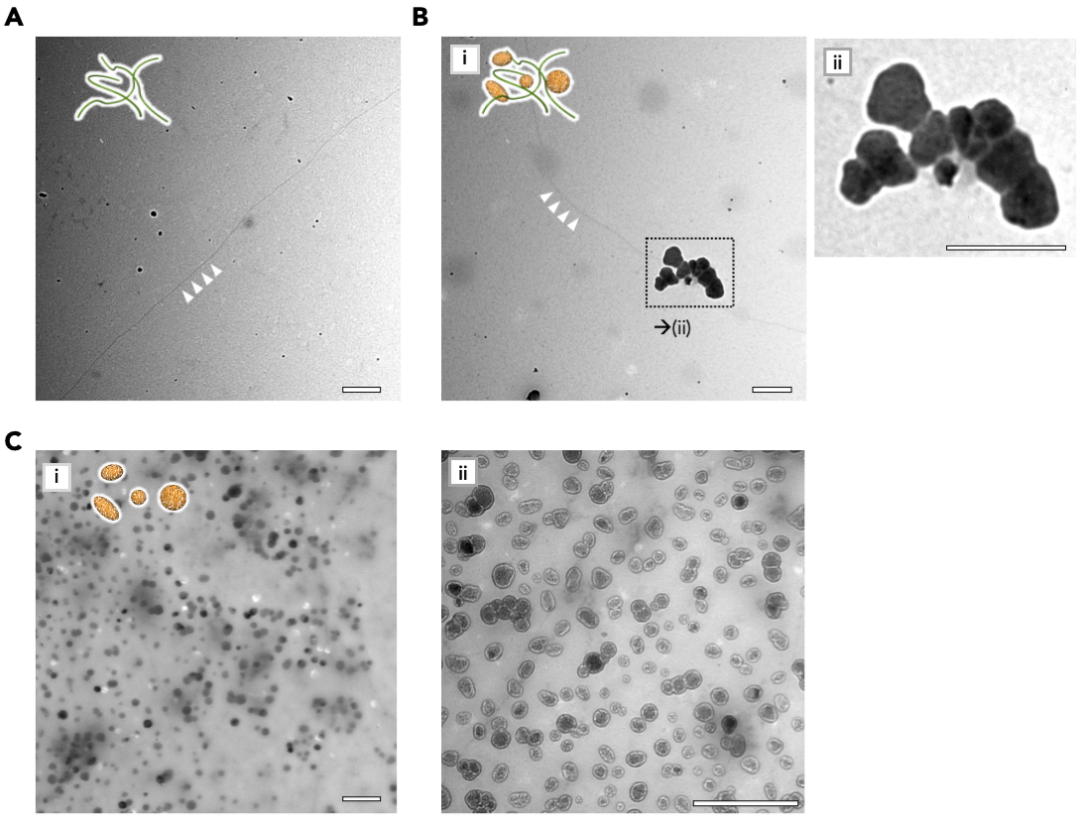

Fig. 8 Representative TEM images showing (**A**) **Z-AF-BPS** nanofibers and DNA nanoflowers constructed by the RCA reaction in (**B**) the presence (during the pre-RCA-mixing protocol, corresponding to **Fig. 7B**) and (**C**) absence of **Z-AF-BPS** nanofibers. Magnified images for (**B**) and (**C**) are shown in panels (**ii**). Fibrous architectures are highlighted using white arrows in panels (**A**) and (**B**). Schematics showing each supramolecular architecture are also presented in the top left corner of the images. Scale bar: 500 nm.

Conclusions

We have successfully constructed multicomponent hybrid supramolecular materials comprising fibrous nanostructures through the self-assembly of peptide derivatives and DNA nanoflowers using the RCA reaction under isothermal conditions. To the best of our knowledge, such orthogonal coexistence of peptide-based supramolecular nanostructures and DNA nanoflowers has not been reported. Furthermore, this study demonstrated the protease-responsive, selective degradation of a peptide-based supramolecular nanofibers

embedded in hybrid supramolecular materials, which additionally suppors the view that each supramolecular architecture was constructed through the orthogonal assembly process from the component bio-related molecules. We believe that this unique supramolecular hybrid (nano)materials could offer a distinct opportunity of exploring bioapplications like cell-culturing or drug-releasing matrices. Research along such lines is in progress in our laboratory.

Conflicts of interest

There are no conflicts to declare.

Acknowledgments

This work was supported in part by a financial support from the Uehara Memorial Foundation, the JSPS Core-to-Core Program, the iGCORE collaboration grant (MI), a Grant-in-Aid for Scientific Research (C) of the Japan Society for the Promotion of Science (20K05563, AS), a JSPS Research Fellowship for Young Scientists (SLH), and a THERS Interdisciplinary Frontier Next Generation Researcher Project (YS). Additionally, we acknowledge the Life Science Research Center, Gifu University, for their kind and continuous support. Finally, the authors thank Enago (www.enago.jp) for the English language review.

Notes and references

1 G. M. Whitesides and M. Boncheva, *Proc. Natl. Acad. Sci. U.S.A.,* **2002**, 99, 4769–4774.

2 J.-M. Lehn, *Angew. Chem. Int. Ed.,* **2013**, 52, 2836–2850.

3 T. Aida, E. W. Meijer and S. I. Stupp, *Science*, **2012**, 335, 813–817.

4 H. Wu and M. Fuxreiter, *Cell*, **2016**, 165, 1055–1066.

5 A. M. Brizard and J. H. van Esch, *Soft Matter*, **2009**, 5, 1320–1327.

6 H. Shigemitsu and I. Hamachi, *Acc. Chem. Res.,* **2017**, 50, 740–750.

7 G. Vantomme and E. W. Meijer, *Science*, **2019**, 363, 1396–1397.

8 S. Yang and L. Jiang, *Chem. Commun.*, **2020**, 56, 8342–8354.

9 I. Insua and J. Montenegro, *Chem*, **2020**, 6, 1652–1682.

10 K. Matsuura, *Chem. Commun.*, **2018**, 54, 8944–8959.

11 T. MacCulloch, A. Buchberger and N. Stephanopoulos, *Org. Biomol. Chem.*, **2019**, 17, 1668–1682.

12 S. L. Higashi, N. Rozi, S. A. Hanifah and M. Ikeda, *Int. J. Mol. Sci.*, **2020**, 21, 9458.

13 S. Liu, P. Du, H. Sun, H.-Y. Yu and Z.-G. Wang, *ACS Catalysis*, **2020**, 10, 14937–14958.

14 C. G. Evans and E. Winfree, *Chem. Soc. Rev.*, **2017**, 46, 3808–3829.

15 M. Madsen and K. V. Gothelf, *Chem. Rev.,* **2019**, 119, 6384–6458.

16 A. Keller and V. Linko, *Angew. Chem. Int. Ed.,* **2020**, 59, 15818–15833.

17 S. L. Higashi, A. Shibata, Y. Kitamura, K. M. Hirosawa, K. G. N. Suzuki, K. Matsuura and M. Ikeda, *Chem. Eur. J.*, **2019**, 25, 11955–11962.

18 S. L. Higashi, K. M. Hirosawa, K. G. N. Suzuki, K. Matsuura and M. Ikeda, *ACS App. Bio Mater.*, **2020**, 3, 9082–9092.

19 K. Matsuura, T. Yamashita, Y. Igami and N. Kimizuka, *Chem. Commun.*, **2003**, 376–377.

20 K. Matsuura, K. Masumoto, Y. Igami, T. Fujioka and N. Kimizuka, *Biomacromolecules*, **2007**, 8, 2726–2732.

21 W. K. P. Rothemund, A. Ekani-Nkodo, N. Papadakis, A. Kumar, K. D. Fygenson and E. Winfree, *J. Am. Chem. Soc.*, **2004**, 126, 16344–16352.

22 J. Lv, Y. Dong, Z. Gu and D. Yang, *Chem. Eur. J.,* **2020**, 26, 14512–14524.

23 M. G. Mohsen and E. T. Kool, *Acc. Chem. Res.*, **2016**, 49, 2540–2550.

24 Y. R Baker, J. Chen, J. Brown, A. H El-Sagheer, P. Wiseman, E. Johnson, P. Goddard and T. Brown, *Nucleic Acids Res.*, **2018**, 46, 7495–7505.

25 T. Sugiura, T. Kanada, D. Mori, H. Sakai, A. Shibata, Y. Kitamura and M. Ikeda, *Soft Matter*, **2020**, 16, 899–906.

26 R. Riek and D. S. Eisenberg, *Nature*, **2016**, 539, 227–235.

27 S. J. T. Van Noort, K. O. Van der Werf, B. G. De Grooth, N. F. Van Hulst and J. Greve, *Ultramicroscopy*, **1997**, 69, 117–127.

28 K. K. M. Sweers, K. O. van der Werf, M. L. Bennink and V. Subramaniam, *ACS Nano*, **2012**, 6, 5952–5960.

29 D. R. Boyer, N. A. Mynhier and M. R. Sawaya, *bioRxiv*, **2021**, 2021.07.02.450971; doi: https://doi.org/10.1101/2021.07.02.450971.

30 T. Ohtomi, S. L. Higashi, D. Mori, A. Shibata, Y. Kitamura and M. Ikeda, *Pept. Sci.*, **2021**, 113, e24200.

31 R. Kubota, K. Nakamura, S. Torigoe and I. Hamachi, *ChemistryOpen,* **2020**, 9, 67–79.

32 D. Shen, J. Coleman, E. Chan, T. P. Nicholson, L. Dai, P. W. Sheppard and W. F. Patton, *Cell Biochem. Biophys.*, **2011**, 60, 173–185.

33 S. Navarro and S. Ventura, *Biotechnology Journal*, **2014**, 9, 1259–1266.

34 M. Pieszka, S. Han, C. Volkmann, R. Graf, I. Lieberwirth, K. Landfester, D. Y. W. Ng and T. Weil, *J. Am. Chem. Soc.,* **2020**, 142, 15780–15789.

35 M. M. Ali, S. Su, C. D. M. Filipe, R. Pelton and Y. Li, *Chem. Commun.*, **2007**, 4459–4461.

36 Y. Zhao, L. Qi, F. Chen, Y. Dong, Y. Kong, Y. Wu and C. Fan, *Chem. Commun.*, **2012**, 48, 3354–3356.

37 G. Zhu, R. Hu, Z. Zhao, Z. Chen, X. Zhang and W. Tan, *J. Am. Chem. Soc.*, **2013**, 135, 16438–16445.

38 Y. Lv, R. Hu, G. Zhu, X. Zhang, L. Mei, Q. Liu, L. Qiu, C. Wu and W. Tan, *Nat. Protoc.*, **2015**, 10, 1508–1524.

39 W. Ebeling, N. Hennrich, M. Klockow, H. Metz, H. D. Orth and H. Lang, *Eur. J. Biochem.*, **1974**, 47, 91–97.

40 K. Nam, T. Kim, Y. M. Kim, K. Yang, D. Choe, L. B. Mensah, K. Y. Choi and Y. H. Roh, *Chem. Commun.,* **2019**, 55, 4905–4908.

41 B. T. Tran, J. Kim and D.-R. Ahn, *Nanoscale*, **2020**, 12, 22945–22951.